BJP British Journal of Pharmacology

DOI:10.1111/bph.13081
www.brjpharmacol.org

RESEARCH PAPER

Seven novel modulators of the analgesic target $Na_V1.7$ uncovered using a high-throughput venom-based discovery approach

Julie K Klint[1], Jennifer J Smith[1], Irina Vetter[1], Darshani B Rupasinghe[1], Sing Yan Er[1], Sebastian Senff[1], Volker Herzig[1], Mehdi Mobli[2], Richard J Lewis[1], Frank Bosmans[3,4] and Glenn F King[1]

[1]*Centre for Pain Research, Institute for Molecular Bioscience,* [2]*Centre for Advanced Imaging, The University of Queensland, St. Lucia, Qld, Australia, and* [3]*Department of Physiology* and [4]*Solomon H. Snyder Department of Neuroscience, School of Medicine, Johns Hopkins University, Baltimore, MD, USA*

Correspondence
Professor Glenn F King or Professor Frank Bosmans, Institute for Molecular Bioscience, The University of Queensland, 306 Carmody Road, St. Lucia, Qld 4072, Australia.
E-mail:
glenn.king@imb.uq.edu.au;
r.lewis@imb.uq.edu.au;
frankbosmans@jhmi.edu

Received
3 July 2014
Revised
8 November 2014
Accepted
8 December 2014

BACKGROUND AND PURPOSE

Chronic pain is a serious worldwide health issue, with current analgesics having limited efficacy and dose-limiting side effects. Humans with loss-of-function mutations in the voltage-gated sodium channel $Na_V1.7$ ($hNa_V1.7$) are indifferent to pain, making $hNa_V1.7$ a promising target for analgesic development. Since spider venoms are replete with Na_V channel modulators, we examined their potential as a source of $hNa_V1.7$ inhibitors.

EXPERIMENTAL APPROACH

We developed a high-throughput fluorescent-based assay to screen spider venoms against $hNa_V1.7$ and isolate 'hit' peptides. To examine the binding site of these peptides, we constructed a panel of chimeric channels in which the S3b-S4 paddle motif from each voltage sensor domain of $hNa_V1.7$ was transplanted into the homotetrameric $K_V2.1$ channel.

KEY RESULTS

We screened 205 spider venoms and found that 40% contain at least one inhibitor of $hNa_V1.7$. By deconvoluting 'hit' venoms, we discovered seven novel members of the NaSpTx family 1. One of these peptides, Hd1a (peptide μ-TRTX-Hd1a from venom of the spider *Haplopelma doriae*), inhibited $hNa_V1.7$ with a high level of selectivity over all other subtypes, except $hNa_V1.1$. We showed that Hd1a is a gating modifier that inhibits $hNa_V1.7$ by interacting with the S3b-S4 paddle motif in channel domain II. The structure of Hd1a, determined using heteronuclear NMR, contains an inhibitor cystine knot motif that is likely to confer high levels of chemical, thermal and biological stability.

CONCLUSION AND IMPLICATIONS

Our data indicate that spider venoms are a rich natural source of $hNa_V1.7$ inhibitors that might be useful leads for the development of novel analgesics.

Abbreviations

Ca_V channel, voltage-gated calcium channel; FLIPR, fluorescence imaging plate reader; Hd1a, peptide μ-TRTX-Hd1a from venom of the spider *Haplopelma doriae*; $hNa_V1.7$, human voltage-gated sodium channel subtype 1.7; ICK, inhibitor cystine knot; K_V channel, voltage-gated potassium channel; MALDI-TOF, matrix-assisted laser desorption/ionization time-of-flight; MBP, maltose binding protein; NaSpTx, spider toxin that targets voltage-gated sodium channels; NaSpTx-F1, NaSpTx family 1; Na_V channel, voltage-gated sodium channel; RMSD, root-mean-square deviation; SAR, structure–activity relationship; TTX, tetrodotoxin

Tables of Links

TARGETS		
Ca_v channels	$Na_v1.2$ channel	$Na_v1.6$ channel
$K_v2.1$ channel	$Na_v1.3$ channel	$Na_v1.7$ channel
$K_v11.1$ (ERG) channel	$Na_v1.4$ channel	$Na_v1.8$ channel
$Na_v1.1$ channel	$Na_v1.5$ channel	$Na_v1.9$ channel

LIGANDS
Glutathione
Tetrodotoxin (TTX)
Veratridine

These Tables list key protein targets and ligands in this article which are hyperlinked to corresponding entries in http://www.guidetopharmacology.org, the common portal for data from the IUPHAR/BPS Guide to PHARMACOLOGY (Pawson *et al.*, 2014) and are permanently archived in the Concise Guide to PHARMACOLOGY 2013/14 (Alexander *et al.*, 2013).

Introduction

Chronic pain is a major health issue worldwide that affects ~15% of the adult population (Gaskin and Richard, 2012). The annual economic burden of chronic pain in the United States is ~$600 billion, which exceeds the combined economic cost of cancer, diabetes and stroke (Gaskin and Richard, 2012). There is an unmet clinical need for more effective analgesics to treat chronic pain as most currently available drugs have limited efficacy and dose-limiting side effects.

Voltage-gated sodium (Na_V) channels are transmembrane proteins that regulate the electrical properties of cells. There are nine mammalian subtypes denoted $Na_V1.1$–$Na_V1.9$ (Catterall *et al.*, 2005). Several remarkable genetic studies led to the emergence of human $Na_V1.7$ ($hNa_V1.7$) as an analgesic target. Gain-of-function mutations in the *SNC9A* gene encoding $hNa_V1.7$ cause painful inherited neuropathies (Yang *et al.*, 2004; Fertleman *et al.*, 2006; Estacion *et al.*, 2008; Cheng *et al.*, 2011; Theile *et al.*, 2011), whereas loss-of-function mutations result in congenital indifference to all forms of pain (Cox *et al.*, 2006). Moreover, single nucleotide polymorphisms in *SCN9A* are associated with differences in pain sensitivity (Reimann *et al.*, 2010; Duan *et al.*, 2013; Reeder *et al.*, 2013). Thus, the combined genetic data suggest that subtype-selective inhibitors of $hNa_V1.7$ are likely to be useful analgesics for treating a broad range of pain conditions (King and Vetter, 2014).

Spider venoms are a rich source of peptidic Na_V channel modulators (Herzig *et al.*, 2011; Gilchrist *et al.*, 2014), which are classified into 12 families of Na_V channel toxins (NaSpTxs) based upon their primary structure and disulfide framework (Klint *et al.*, 2012). Most NaSpTxs are gating modifiers that perturb channel function by stabilizing one or more voltage sensors in a particular state (Gilchrist *et al.*, 2014). Since the voltage sensors are less conserved than the pore region of Na_V channels, these toxins have the potential to selectively modulate particular Na_V channel subtypes.

Spiders are the most successful group of venomous animals, with >45 000 extant species. Their venoms contain hundreds to thousands of peptides (Escoubas *et al.*, 2006), with even a conservative estimate of 200 peptides per venom, leading to a total of 9 million spider-venom peptides. Thus far, only ~0.01% of this vast pharmacological landscape has been explored, providing massive scope for discovery of novel Na_V channel modulators from these arachnids. Here, we describe a high-throughput pipeline for the discovery and characterization of $hNa_V1.7$ modulators from spider venoms. We report seven novel peptides from NaSpTx family 1 (NaSpTx-F1) discovered using this approach, and use one of these peptides to exemplify high-throughput methods we developed for determining their structure and Na_V channel binding site. We anticipate that development of detailed structure–function relationships for members of NaSpTx-F1, including the seven peptides described here, will facilitate the engineering of selective inhibitors of $hNa_V1.7$ that might be useful analgesics.

Methods

High-throughput screen of spider venoms against $hNa_V1.7$

Mild electrical currents were applied to the chelicerae of spiders to stimulate venom secretion. Venom was collected in polypropylene tubes, lyophilized and stored at –20°C until required. Venoms and venom fractions were assessed against $hNa_V1.7$ endogenously expressed in SH-SY5Y neuroblastoma cells (Vetter *et al.*, 2012). Briefly, SH-SY5Y cells were maintained at 37°C/5% CO_2 in RPMI containing 15% FBS and 2 mM L-glutamine and seeded on black-walled 96- or 384-well imaging plates at a density of 30 000 or 150 000 cells per well. After 48 h, cells were loaded for 30 min at 37°C with Calcium 4 No-Wash dye (Molecular Devices, Sunnyvale, CA, USA) diluted in physiological salt solution [composition (in mM) NaCl 140, glucose 11.5, KCl 5.9, $MgCl_2$ 1.4, NaH_2PO_4

1.2, $NaHCO_3$ 5, $CaCl_2$ 1.8, HEPES 10]. Ca^{2+} responses following addition of veratridine (50 μM) were measured using a fluorescence imaging plate reader ($FLIPR^{TETRA}$; Molecular Devices) (excitation 470–495 nm, emission 515–575 nm) after 5 min pre-incubation with venom or venom fractions. Under these conditions, most of the veratridine-induced response is mediated by $hNa_V1.7$, with smaller contributions from $hNa_V1.2$ and $hNa_V1.3$ (Vetter *et al.*, 2012).

Isolation of $Na_V1.7$ inhibitors. Venom (1 mg) was diluted with H_2O, filtered (Ultrafree-MC Centrifugal Filter, 0.22 μm; Merck Millipore, Bayswater, Vic, Australia) and then loaded onto an analytical C_{18} reverse-phase (RP) HPLC column (Vydac 4.6 × 250 mm, 5 μm; Grace, Columbia, MD, USA) attached to a Prominence HPLC system (Shimadzu, Rydalmere, NSW, Australia). Components were eluted at 1 mL·min^{-1} with solvent A [99.5% H_2O, 0.05% trifluoroacetic acid (TFA)] and solvent B (90% CH_3CN, 0.05% TFA in H_2O) using isocratic elution at 5% solvent B for 5 min, followed by a gradient of 5–20% solvent B over 5 min, then 20–40% solvent B over 40 min and then 40–80% solvent B over 5 min (or minor variations of this gradient). $hNa_V1.7$-active fractions were further fractionated using a polysulfoethyl cation exchange column (4.6 × 100 mm, 3 μm, 300 Å pore size) and eluted at 1 mL·min^{-1} with solvent A [KH_2PO_4, 20% (v/v) CH_3CN, pH 2.7] and solvent B (1 M KCl in solvent A) using a gradient of 0–50% solvent B over 50 min. Absorbance was measured at 214 and 280 nm using a Shimadzu Prominence SPD-20A detector.

Sequencing of $Na_V1.7$-active peptides. Peptide masses were determined using matrix-assisted laser desorption/ionization time-of-flight (MALDI-TOF) MS using a Model 4700 Proteomics Analyser (Applied Biosystems, Foster City, CA, USA). HPLC fractions were spotted with α-cyano-4-hydroxycinnamic acid (5 mg·mL^{-1} in 50% CH_3CN). Peptides were reduced and alkylated before being sequenced. Disulfide bonds were reduced by incubating peptides for 15 min at 65°C in 150 mM Tris (pH 8), 1 mM EDTA and 5 mM DTT. Thiol groups were pyridylethylated using 5 μL of 95% 4-vinylpyridine and 20 μL of CH_3CN; the reaction was allowed to proceed for 2 h in darkness at room temperature (RT). Both reactions were performed under N_2. Samples were desalted using RP-HPLC (C_{18} column, 2.1 × 100 mm, 5 μm; Thermo Scientific, Waltham, MA, USA) and eluted in solvent B (5% for 15 min, 5–40% over 35 min, 40–80% over 10 min, 0.25 mL·min^{-1}). Reaction progress was monitored using MS. N-terminal sequencing was performed by the Australian Proteome Analysis Facility.

Production of recombinant Hd1a. A synthetic gene encoding Hd1a (peptide μ-TRTX-Hd1a from the venom of the spider *Haplopelma doriae*), with codons optimized for *Escherichia coli* expression, was cloned into the pLic-MBP (maltose binding protein) vector (Cabrita *et al.*, 2006). This plasmid, which enables periplasmic production of a His_6-MBP-Hd1a fusion protein, was transformed into *E. coli* strain BL21(λDE3) for Hd1a production. Cultures were grown in Luria-Bertani medium at 37°C with shaking at 180 r.p.m. When the OD_{600} reached 0.8–1.0, the culture was cooled to 16°C and induced with 1 mM isopropyl b-D-1-thiogalactopyranoside (IPTG). Cells were harvested 12–14 h later by centrifugation for 15 min at 8000× *g*. For production of uniformly $^{13}C/^{15}N$-labelled Hd1a, cultures were grown in minimal medium supplemented with $^{13}C_6$-glucose and $^{15}NH_4Cl$ as the sole carbon and nitrogen sources respectively. Cells were disrupted under constant pressure at 30 kPa (TS Series Cell Disrupter, Constant Systems, Northants, UK), then the His_6-MBP-toxin fusion protein was captured on Ni-NTA Superflow resin (Qiagen, Valencia, CA, USA). The resin was washed with 15 mM imidazole to remove non-specifically bound proteins and then fusion protein was eluted with 500 mM imidazole. After buffer exchange to remove imidazole, reduced and oxidized glutathione were added to 0.6 and 0.4 mM, respectively, to activate TEV protease and promote peptide folding. After the addition of His_6-tagged TEV protease (~40 μg·mg^{-1} Hd1a), cleavage was allowed to proceed at RT for 12 h. His_6-MBP and His_6-TEV protease were precipitated with TFA (1%), then Hd1a was purified from the supernatant using RP-HPLC (C_4 column; 250 × 10 mm, 5 μm; flow rate 3 mL·min^{-1}; Phenomenex, Torrance, CA, USA) with a gradient of 10–60% solvent B (0.43% TFA in 90% acetonitrile) in solvent A (0.5% TFA in water) over 50 min. If required, a final purification was performed (Aquasil C_{18} column, 150 × 4.6 mm, 5 μm; flow rate 1 mL·min^{-1}) using a gradient of 25–30% solvent B over 20 min.

Construction of $hNa_V1.7/K_V2.1$ chimeras. Channel chimeras were generated using sequential PCR with $K_V2.1\Delta7$ (Frech *et al.*, 1989; Swartz and MacKinnon, 1997) and $hNa_V1.7$ (Origene Technologies, Rockville, MD, USA) as templates. The $K_V2.1\Delta7$ construct contains seven-point mutations in the outer vestibule that render the channel sensitive to agitoxin-2, a pore-blocking scorpion toxin (Garcia *et al.*, 1994). cRNA was synthesized using T7 polymerase (mMessage mMachine kit; Life Technologies, Federick, MD, USA) after linearizing DNA with appropriate restriction enzymes.

Electrophysiology. *Xenopus laevis* oocytes were injected with cRNA encoding hNa_V α and β1 subunits, $K_V2.1$, $K_V2.1$/$hNa_V1.7$ chimeras, or $K_V2.1$/$hNa_V1.9$ chimeras. Two-electrode voltage-clamp electrophysiology (OC-725C, Warner Instruments, Hamden, CT, USA; 150 μL recording chamber) was used to measure currents 1–4 days after cRNA injection and incubation at 17°C in ND96 that contained (in mM) 96 NaCl, 2 KCl, 5 HEPES, 1 $MgCl_2$, 1.8 $CaCl_2$ and 50 μg·mL^{-1} gentamycin, pH 7.6. Data were filtered at 4 kHz and digitized at 20 kHz using pClamp software (Molecular Devices). Microelectrode resistances were 0.5–1 MΩ when filled with 3 M KCl. For K_V channel experiments, the external recording solution contained (in mM) 50 KCl, 50 NaCl, 5 HEPES, 1 $MgCl_2$, 0.3 $CaCl_2$, pH 7.6 with NaOH. For Na_V channel experiments, the external recording solution contained (in mM) 96 NaCl, 2 KCl, 5 HEPES, 1 $MgCl_2$, 1.8 $CaCl_2$, pH 7.6 with NaOH. All experiments were performed at RT (~22 °C). Toxin samples were diluted in recording solution with 0.1% BSA. Leak and background conductance, identified by blocking channels with agitoxin-2 or tetrodotoxin (TTX), were subtracted for all K_V or $hNa_V1.7$ currents respectively.

Voltage–activation relationships were obtained by measuring tail currents for K_V channels or by monitoring steady-state currents and calculating conductance for Na_V channels. Occupancy of closed or resting channels by toxins was examined using negative holding voltages where the open probability was very low, and the fraction of unbound

channels was estimated using depolarizations too weak to open toxin-bound channels. After the addition of toxin to the recording chamber, equilibration between toxin and channel was monitored using weak depolarizations elicited at 5–10 s intervals. For all channels, voltage–activation relationships were recorded in the absence and presence of toxin. Off-line data analysis was performed using Clampfit (Molecular Devices) and Origin 7.5 (Originlab, Northampton, MA, USA).

Determination of Hd1a structure. $^{13}C/^{15}N$-labelled Hd1a (500 μM in 20 mM sodium acetate buffer containing 5% D_2O, pH 4.9) was filtered (Ultrafree-MC 0.22 μm centrifugal filter; Merck Millipore) and then 300 μL was added to a susceptibility-matched microtube (Shigemi, Allison Park, PA, USA). Data were acquired at 25°C on a 900 MHz NMR spectrometer (Bruker Biospin, Ettlingen, Germany) equipped with a cryogenic probe. Spectra used for resonance assignments were acquired using non-uniform sampling (NUS) (Mobli *et al.*, 2010). NUS data were processed using the Rowland NMR toolkit with automatic selection of maximum entropy parameters (Mobli *et al.*, 2007). ^{13}C- and ^{15}N-edited HSQC-NOESY experiments (mixing time 200 ms) were acquired with uniform sampling. Dihedral angles were derived using TALOS+ (Shen *et al.*, 2009); restraint ranges for structure calculations were set to twice the estimated SD. NOESY spectra were manually peak picked and integrated, then peak lists were automatically assigned, distance restraints extracted and structures calculated using CYANA 3.0 (Güntert, 2004).

Results

Screening spider venoms for hNa$_V$1.7 modulators

For this assay, we utilized a human cell line (SH-SY5Y) that expresses high levels of hNa$_V$1.7 (Vetter *et al.*, 2012). Activation of hNa$_V$1.7 with veratridine leads to membrane depolarization, which activates endogenous voltage-gated calcium (Ca$_V$) channels (Sousa *et al.*, 2013). The resultant influx of calcium ions induces a fluorescence response when they bind internalized Calcium 4 dye (see control wells 1A–1H and 12A–12H in Figure 1A). Due to the large cellular Ca^{2+} gradient and the comparatively high sensitivity of calcium dyes, this method yields better signal-to-noise ratio than alternative approaches, including membrane potential or Na^+-specific dyes. We utilized a two-addition protocol in which spider venoms (0.4–20.0 μg) and subsequently veratridine were added to the wells of a 96-well plate, and used this assay to screen for hNa$_V$1.7 modulators. Venoms with putative Na$_V$1.7 inhibitors caused a loss of the veratridine-induced fluorescent signal (e.g., wells 2A, 3E, 5F in Figure 1A). In contrast, putative activators were characterized by a spontaneous increase in fluorescence prior to addition of veratridine (e.g., wells 2G and 7B). Some venoms appear to contain both activators and inhibitors of Na$_V$1.7 as they induced a fluorescent signal prior to veratridine addition and also blocked the veratridine-induced response (e.g., well 3G). Since spider venoms are also a rich source of Ca$_V$ channel modulators (King, 2007; King *et al.*, 2008a), some venoms might contain molecules that abrogate the fluorescent response due block of Ca$_V$ rather than Na$_V$ channels. Modulation of hNa$_V$1.7 by crude venoms could also be due to the synergistic effect of multiple compounds, an effect that might be lost upon venom fractionation.

We used this assay to screen venoms from 205 spiders belonging to 13 different taxonomic families (Supporting Information Table S1). Eighty-two venoms (40%) inhibited the fluorescent response and therefore putatively contain at least one inhibitor of hNa$_V$1.7, whereas 30 venoms (14.6%) caused a spontaneous increase in fluorescence and therefore putatively contain at least one activator of

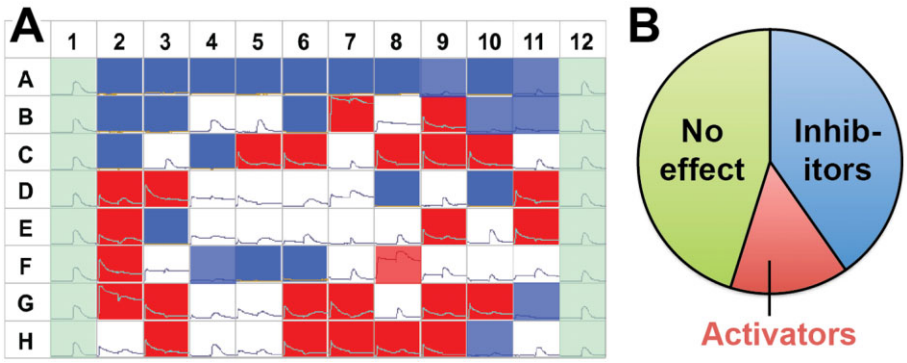

Figure 1

High-throughput screen of spider venoms against hNa$_V$1.7. (A) Example of a 96-well plate from a FLIPR-based screen of spider venoms against hNa$_V$1.7 endogenously expressed in SH-SY5Y cells. Wells 1A–1H and 12A–12H (pale green) were buffer controls showing the fluorescent response obtained when hNa$_V$1.7 was activated by veratridine. All other wells contained spider venoms. Wells containing venoms that inhibited the veratridine-induced fluorescent response are highlighted in blue, whereas wells containing venoms that elicited a fluorescence response before the addition of veratridine and thus putatively contain activators of hNa$_V$1.7 are highlighted in red. (B) Statistics of venom screen. Eighty-two of the 205 spider venoms inhibited the fluorescent response and therefore putatively contain inhibitors of hNa$_V$1.7, whereas 30 venoms caused a spontaneous increase in fluorescence, suggesting that they contain activators of hNa$_V$1.7. Some venoms caused a spontaneous increase in fluorescence as well as a subsequent reduction in the veratridine-induced fluorescent response (e.g. well G3), and hence they putatively contain both activators and inhibitors of hNa$_V$1.7. For the statistical analysis, these venoms were counted only as inhibitors; hence, the number of activators might be higher than indicated here.

$hNa_V1.7$ (Figure 1B). Crude venoms that potently inhibited $hNa_V1.7$ were fractionated using RP-HPLC and then individual fractions were tested in the FLIPR assay. Active fractions were purified to single components (peptides) using an orthogonal ion-exchange chromatography step. These peptides were reduced, alkylated and sequenced using Edman degradation. Using this approach, 15 novel peptides were isolated from eight venoms. Seven peptides were found to be members of NaSpTx-F1 and they will be described here.

Novel members of NaSpTx-F1

As for all previously described NaSpTx-F1 members, the seven new peptides were isolated from theraphosid (tarantula) venoms. Toxins were named based upon the rational nomenclature proposed for spider-venom peptides (King *et al.*, 2008b), with the μ prefix denoting inhibition of Na_V channels. Although it is possible that some of these toxins might inhibit Ca_V rather than Na_V channels, this seems unlikely since all NaSpTx-F1 toxins characterized to date exclusively target Na_V channels (Klint *et al.*, 2012).

Figure 2 outlines purification of the seven peptides, while their amino acid sequences are provided in Table 1. Each peptide comprises 32–35 residues with six cysteine residues that form three disulfide bonds based upon mass of the reduced and oxidized peptides. We did not experimentally determine their disulfide connectivity since, based upon sequence homology, it is presumably the same as previously characterized NaSpTx-F1 members that all contain an inhibitor cystine knot (ICK) with cysteine connectivity C1–C4, C2–C5, C3–C6 (Pallaghy *et al.*, 1994). As shown in Table 1, there is a good agreement between the molecular mass of the native toxins determined using MALDI-TOF MS and the mass calculated from the amino acid sequence. Thus, none of the peptides are C-terminally amidated or contain any other post-translational modification aside from disulfide bonds. Despite the fact that all seven peptides belong to NaSpTx-F1, their sequence similarity is only moderate (38–62% sequence identity with respect to Hd1a; see Table 1). μ-TRTX-Ccy1a and μ-TRTX-Ccy1b are paralogues isolated from the same venom that differ only at position 6 (Ile6 in Ccy1a, Phe6 in Ccy1b).

The seven spider-venom peptides are similar to several previously described members of NaSpTx-F1. μ-TRTX-Cc1a/b, μ-TRTX-Se1a and μ-TRTX-Osp1b are most similar to κ-TRTX-Gr4a (82, 55 and 55% identity, respectively) and β-TRTX-Cm1a (76, 52 and 58% identity, respectively). κ-TRTX-Gr4a (VSTX3) binds to the voltage sensor domain of the archaebacterial voltage-gated potassium channel K_VAP (Ruta and MacKinnon, 2004) but it has not been tested against Na_V channels. β-TRTX-Cm1a (ceratotoxin-1) was isolated based upon its ability to inhibit mammalian Na_V channels; it potently inhibits $Na_V1.1$, $Na_V1.2$, $Na_V1.4$ and $Na_V1.5$ with IC_{50} values ranging from 3 to 890 nM (Bosmans *et al.*, 2006). μ-TRTX-Hd1a (Hd1a), μ-TRTX-Osp1a and μ-TRTX-Ep1a are most similar to μ-TRTX-Hhn1b (hainantoxin-IV, Hhn1b) (82, 62 and 51% identity, respectively), a potent inhibitor of TTX-sensitive Na_V currents in dorsal root ganglion (DRG) neurons (Liu *et al.*, 2012).

Recombinant Hd1a preferentially inhibits $hNa_V1.7$

In order to validate the ability of the FLIPR assay to identify inhibitors of $hNa_V1.7$, we undertook detailed structure–function characterization of Hd1a. Hd1a was produced in the periplasm of *E. coli* to facilitate disulfide bond formation (Klint *et al.*, 2013). The His_6-MBP-Hd1a fusion protein, which was the major cellular protein produced after IPTG induction (Figure 3A, inset), was purified using nickel affinity chromatography, then Hd1a was liberated from the fusion protein with TEV protease and purified using RP-HPLC (Figure 3A). Hd1a was purified to >98% homogeneity as judged by RP-HPLC (Figure 3B) and MS (Figure 3C). In order to facilitate TEV protease cleavage of the His_6-MBP-Hd1a fusion protein, Hd1a was produced with an additional N-terminal glycine residue, the preferred P1′ residue in the TEV protease recog-

Table 1

Amino acid sequences of $hNa_V1.7$-active peptides discovered in this study

Venom	Toxin name	Sequence	Observed mass (Da)	Calculated mass (Da)	Identity (%)
Haplopelma doriae	μ-TRTX-Hd1a	-ACLGFGKSCNPSNDQCCKSSSLACSTKHKWCKYEL	3819.9	3819.7	100
Chromatopelma cyaneopubescens	μ-TRTX-Ccy1a	DDCLGIFKSCNPDNDKCCES--YKCSRRDKWCKYVL	4027.0	4027.8	62
Chromatopelma cyaneopubescens	μ-TRTX-Ccy1b	DDCLGFFKSCNPDNDKCCEN--YKCNRRDKWCKYVL	4115.6	4115.8	59
Orphnaecus species 1[1]	μ-TRTX-Osp1a	-GCKGFGKACKYGADECCKN--LVCSKKHKWCKYTL	3692.5	3692.8	60
Orphnaecus species 2[1]	μ-TRTX-Osp1b	-ECLGWMKGCEPKNNKCC--SSYVCTYKYPWCRYDL	3963.5	3963.7	56
Euathlus pulcherrimaklaasi	μ-TRTX-Ep1a	-DCLKFGWKCNPRNDKCC--SGLKCGSNHNWCKLHL	3800.8	3800.7	50
Selenocosmia effera	μ-TRTX-Se1a	-DCLGWMAGCDFNDNKCC--AGYVCK-KHPWCRYDL	3707.9	3707.5	38

Masses are monoisotopic masses, either determined experimentally using MALDI-TOF MS or calculated using PeptideMass (http://web.expasy.org/peptide_mass/). % identity was calculated relative to Hd1a.

[1]*Orphnaecus* species 1 and 2 were collected from Sibaliw and Maanghit Caves, respectively, on Panai Islands in the Philippines. We have tentatively assumed that these are the same species, and the toxins have been named accordingly.

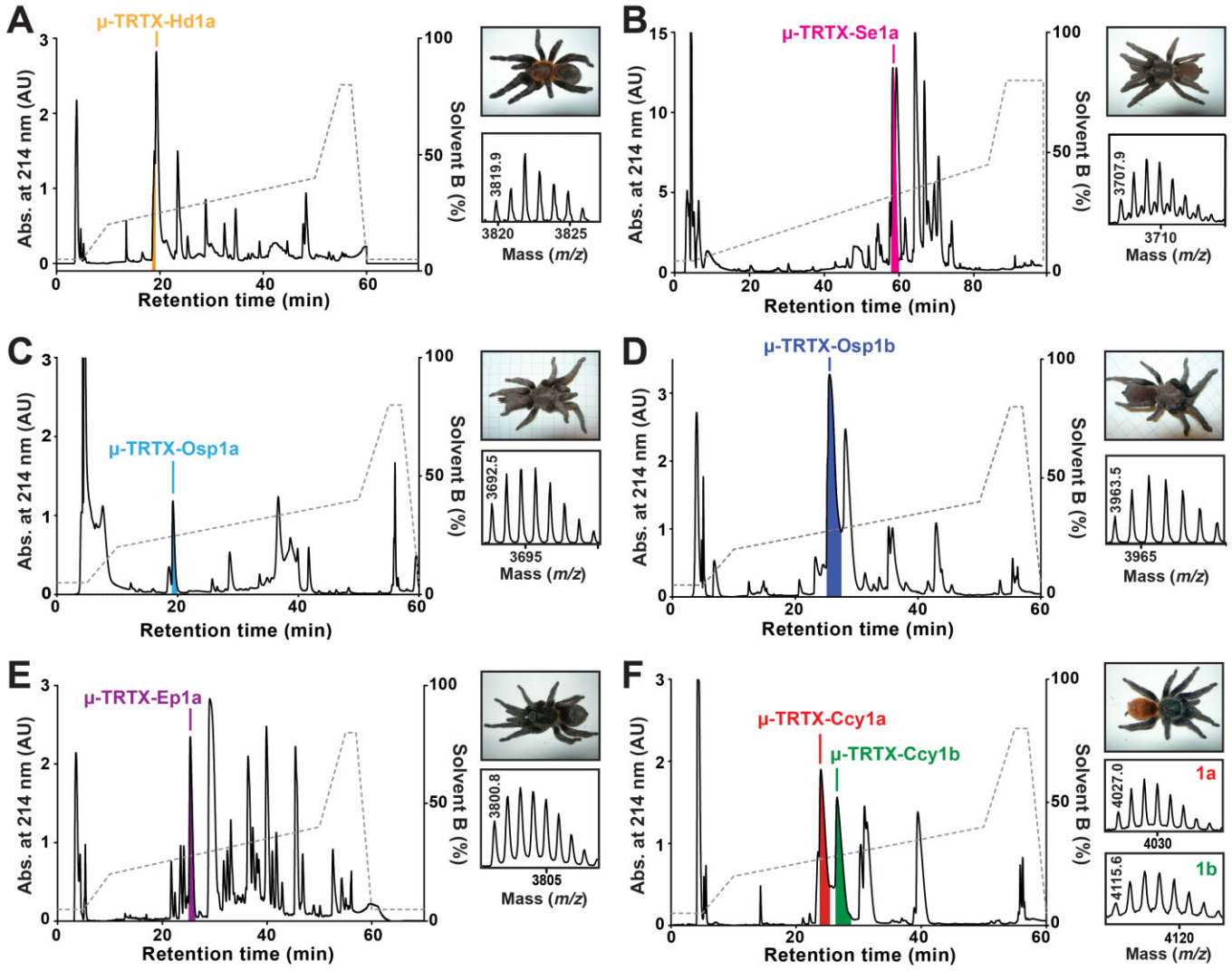

Figure 2

Isolation of novel $Na_V1.7$ inhibitors from spider venom. Each panel shows a chromatogram resulting from fractionation of crude venom using RP-HPLC; the acetonitrile gradient is indicated by the dotted line. Coloured fractions are those that putatively contain inhibitors of $Na_V1.7$. These fractions were further purified using ion exchange chromatography to obtain pure, active peptides. The top inset in each panel shows a photo of the spider from which venom was obtained. The bottom inset in each panel is a MALDI-TOF MS spectrum showing the M + H^+ ion for the purified active peptide. These six panels show isolation of (A) μ-TRTX-Hd1a from the venom of *Haplopelma doriae*; (B) μ-TRTX-Se1a from the venom of *Selenocosmia effera*; (C) μ-TRTX-Osp1a from the venom of *Orphnaecus* species 1; (D) μ-TRTX-Osp1b from the venom of *Orphnaecus species 2;* (E) μ-TRTX-Ep1a from the venom of *Euathlus pulcherrimaklaasi*; (F) μ-TRTX-Ccy1a and μ-TRTX-Ccy1b from the venom of *Chromatopelma cyaneopubescens*.

nition site (Kapust *et al.*, 2002; Renicke *et al.*, 2013); all remaining work was completed with this recombinant toxin (rHd1a).

Application of 1 μM rHd1a caused almost complete inhibition of $hNa_V1.7$-mediated currents recorded from oocytes (Figure 4A). Fitting the Hill equation to concentration–response data (Figure 4B) yielded an IC_{50} of 111 ± 7 nM and a Hill coefficient of 0.95 ± 0.06, indicative of a single toxin binding site. Conductance–voltage (*G-V*) relationships obtained before and after addition of a non-saturating concentration of rHd1a (50 nM) revealed no significant shift in activation (Figure 4C), and inhibition was not voltage-dependent over the range of –25 to 0 mV (Supporting Information Fig. S1A). While this suggests a pore-blocking mechanism of action, additional experiments designed to determine the Hd1a binding site (described below) indicate this is not the case. Hd1a had no effect on steady-state inactivation (Figure 4D) or recovery from inactivation (Figure 4E), and it caused only a minor increase in inactivation time constants (Supporting Information Fig. S2). Inhibition by Hd1a is reversible as $hNa_V1.7$ currents recovered quickly following washout in toxin-free solution (Figure 4F).

The subtype selectivity of rHd1a was assessed by examining its ability to inhibit a complete panel of hNa_V channel

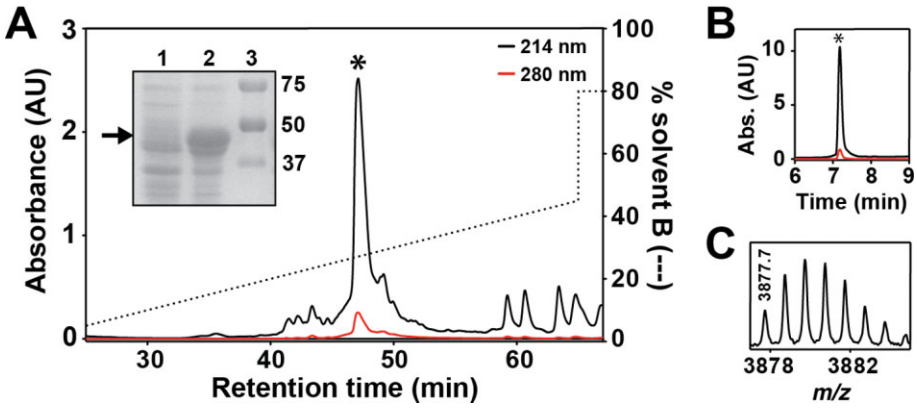

Figure 3

Expression and purification of recombinant Hd1a. (A) RP-HPLC chromatogram showing purification of recombinant Hd1a after cleavage from the His_6-MBP fusion tag by TEV protease. The peak corresponding to Hd1a is highlighted with an asterisk. Inset: SDS-PAGE gel showing *Escherichia coli* cells before (lane 1) and after (lane 2) induction of Hd1a expression with IPTG. Lane 3 contains molecular mass standards, with masses indicated in kDa on the right of the gel. The arrow indicates the running position of the MBP-toxin fusion protein. (B) RP-HPLC chromatogram of recombinant Hd1a after purification, showing a single uniform peak. (C) MALDI-TOF MS spectrum showing the M + H^+ ion for purified recombinant Hd1a (observed, 3877.77 Da; calculated, 3877.71 Da).

subtypes expressed in oocytes, including the key off-target subtypes $hNa_V1.4$, $hNa_V1.5$ and $hNa_V1.6$ (Figure 4G). At a concentration of 1 μM, Hd1a was highly selective with no inhibition of $hNa_V1.5$ or $hNa_V1.8$, 23–31% inhibition of $hNa_V1.3$, $hNa_V1.4$ and $hNa_V1.6$, moderate inhibition of $hNa_V1.2$ (55%), and robust inhibition of $hNa_V1.1$ (87%) and $hNa_V1.7$ (87%) (Figure 4D). Moreover, this selectivity pattern was maintained over a large voltage range (from –25 to 0 mV; Supporting Information Fig. S1B). Hd1a was inactive against hERG ($K_v11.1$ channels; Supporting Information Fig. S3).

Hd1a interacts with domain II voltage sensor of $hNa_V1.7$

The Na_V channel binding site has been examined for only one member of NaSpTx-F1, namely huwentoxin-IV (μ-TRTX-Hh2a, Hh2a), which binds to the S3b-S4 helix-turn-helix motif in the domain II voltage sensor (Xiao *et al.*, 2008). This so-called paddle motif (Alabi *et al.*, 2007; Bosmans *et al.*, 2008) is targeted by a variety of animal toxins. In order to determine whether rHd1a also binds to the paddle region, we transplanted the S3b-S4 paddle motif from each of the four voltage-sensor domains of $hNa_V1.7$ into the homotetrameric $K_V2.1$ channel (Figure 5). For domains (D) I, III and IV of $hNa_V1.7$, we generated functional chimeras using previously described paddle-motif boundaries (Bosmans *et al.*, 2008; 2011) (Figure 5B and C). In the case of DII, we could only record ionic currents when four N-terminal residues were not transferred (Figure 5B and C). Nonetheless, the transferred region in all functional chimeras contained the crucial basic residues that contribute to gating charge movement in K_V channels (Aggarwal and MacKinnon, 1996; Seoh *et al.*, 1996), suggesting that the four voltage-sensing domains in $hNa_V1.7$ contain paddle motifs that are involved in sensing membrane voltage changes.

Examination of the *G-V* relationships for the $hNa_V1.7/K_V2.1$ chimeras revealed that each voltage-sensor paddle has a distinct effect on $K_V2.1$ gating; the midpoints of the *G-V* relations are ≥50, 44 ± 1, –16 ± 2 and 9 ± 1 mV for the DI, II, III and IV constructs respectively (Figure 5D). The voltage sensor in DIV plays a crucial role in fast inactivation, possibly due to its slower response to changes in membrane voltage compared with DI–III and its coupling to the inactivation gate (Sheets *et al.*, 1999; Horn *et al.*, 2000; Chanda and Bezanilla, 2002). The DIV paddle motifs within $rNa_V1.2$ and $rNa_V1.4$ delay channel opening when transplanted into K_V channels, suggesting that this region helps determine the slower kinetics of DIV voltage-sensor activation (Bosmans *et al.*, 2008). To explore whether the DIV paddle motif serves a similar role in $hNa_V1.7$, we measured the kinetics of activation and deactivation of the four chimeras in response to membrane depolarization and repolarization respectively (Figure 5E). As observed for previously studied chimeric channels, the kinetics for the DIV $hNa_V1.7/K_V2.1$ chimera were slower compared with other $hNa_V1.7/K_V2.1$ chimeras, suggesting that the paddle motif in domain IV contributes to fast inactivation in $hNa_V1.7$.

We next examined the effect of rHd1a on $K_V2.1$ and the $hNa_V1.7/K_V2.1$ paddle chimeras. One micromolar rHd1a had no effect on wild-type $K_V2.1$ or the DI, DIII and DIV chimeras, but it strongly inhibited K^+ currents mediated by the DII $hNa_V1.7/K_V2.1$ chimera (Figure 5F). We conclude that rHd1a inhibits $hNa_V1.7$ primarily by interacting with the S3b-S4 paddle in DII.

Since $hNa_V1.9$ has proven recalcitrant to heterologous expression, we also examined the effect of rHd1a on a panel of previously described $hNa_V1.9/K_V2.1$ paddle chimeras in which the S3b-S4 paddle motifs of $hNa_V1.9$ were transplanted into $K_V2.1$ (Bosmans *et al.*, 2011). rHd1a had no effect on currents mediated by any of these chimeras (Supporting Information Fig. S4). Since the transplanted S3b-S4 paddle region encompasses the binding site for rHd1a on $hNa_V1.7$, we tentatively concluded that rHd1a has no effect on $hNa_V1.9$.

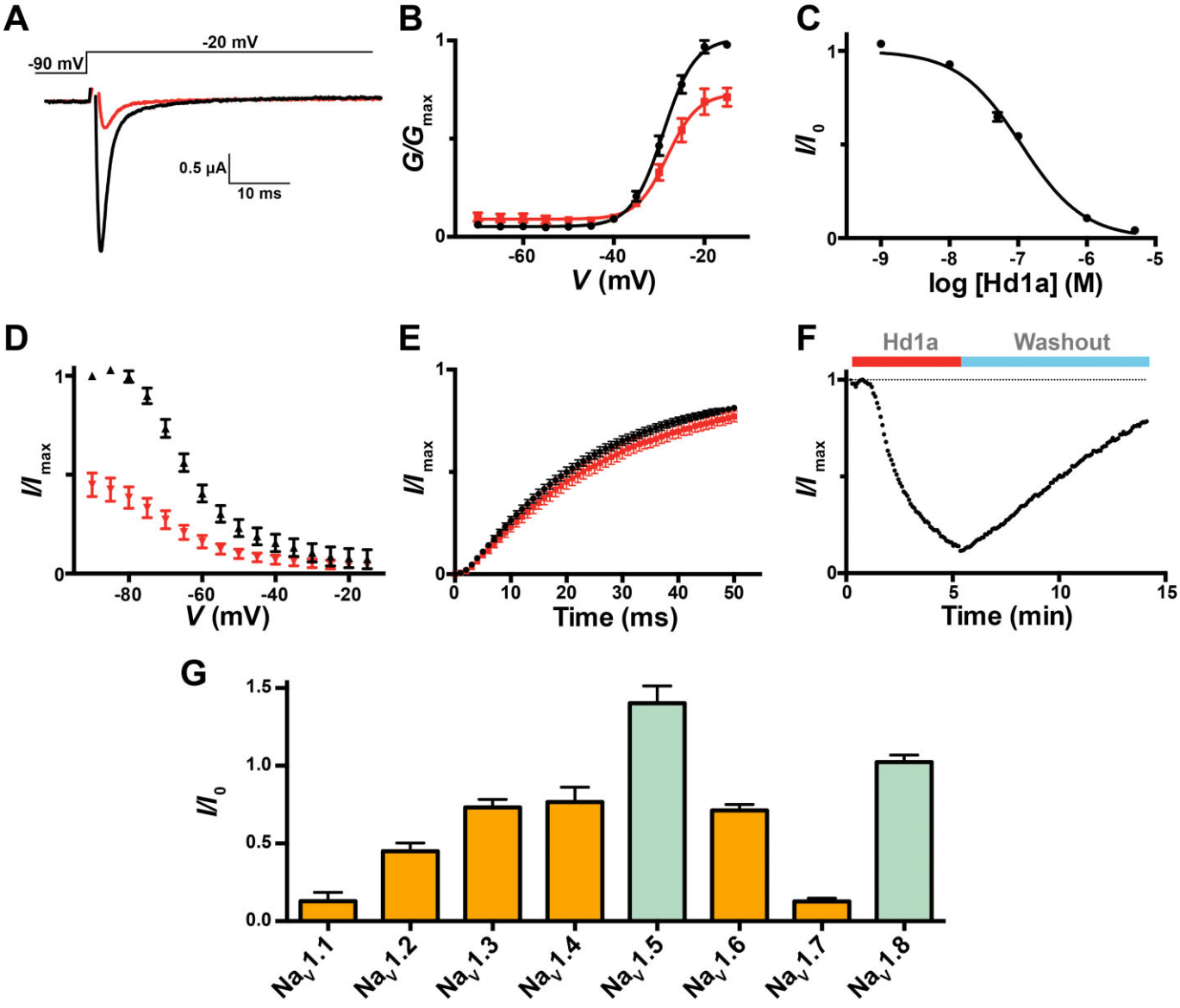

Figure 4

Effect of rHd1a on hNa$_V$1.7/β1. Currents were recorded from *Xenopus* oocytes using the two-electrode voltage-clamp technique. (A) Sodium currents before (black) and after (red) addition of 1 µM rHd1a. (B) Current–voltage relationship before (black) and after (red) addition of 50 nM rHd1a. Currents were evoked from a holding potential of –90 mV, stepping from –70 to –10 mV in 5 mV increments. (C) I/I_0 as a function of rHd1a concentration (n = 3–4; error bars represent SEM). Fitting the Hill equation to the data yielded an IC_{50} of 111 ± 7 nM and Hill coefficient of 0.95 ± 0.06. (D) Steady-state fast inactivation before (black) and after (red) addition of 1 µM rHd1a. Currents were evoked from a holding potential of –90 mV stepping to –15 mV in 5 mV increments. (E) Recovery from fast inactivation before (black) and after (red) addition of 1 µM rHd1a. Currents were evoked from a holding potential of –90 mV by applying a –15 mV pulse followed by repolarization to–90 mV. A second pulse to –15 mV was applied after a period ranging from 0 to 50 ms, increasing in 1 ms increments. (F) hNa$_V$1.7 currents (I/I_{max}) following application of 1 µM rHd1a for 5 min followed by washout for 10 min. Depolarizing pulses were applied from –90 to –20 mV every 80 ms. (G) Selectivity of rHd1a. hNa$_V$1 currents (I/I_0) in the presence of 1 µM rHd1a (n = 3–4; error bars denote SEM). Orange and green bars denote TTX-sensitive and TTX-resistant hNa$_V$ subtypes respectively. All currents were evoked by a depolarization to –20 mV from a holding potential of –90 mV.

Solution structure of rHd1a

The bacterial expression system described earlier allowed production of uniformly $^{13}C/^{15}N$-labelled Hd1a for structure determination using NMR. ^1H_N, ^{15}N, $^{13}C'$, $^{13}C\alpha$, $^{13}C\beta$ resonance assignments for Hd1a were obtained by analysing amide-proton strips in three-dimensional (3D) HNCACB, CBCA-(CO)NH and HNCO spectra. Additional side chain chemical shifts were obtained from $^{15}N/^{13}C$-NOESY spectra and a four-dimensional (4D) HCC(CO)NH-TOCSY experiment that provides side chain ^1H-^{13}C connectivities (Mobli *et al.*, 2010). An assigned two-dimensional (2D) ^1H-^{15}N HSQC spectrum of rHd1a is shown in Supporting Information Fig. S5, and

complete chemical shifts are available from BioMagResBank (accession number 19998). CYANA 3.0 was used to automatically assign NOESY spectra and calculate 200 structures from random starting conformations; the 20 structures with best stereochemical quality as judged by MolProbity (Chen *et al.*, 2010) were selected to represent the structure of rHd1a (PDB ID 2MPQ; Figure 6).

Statistics highlighting the high precision and stereochemical quality of the ensemble of rHd1a structures are shown in Table 2. The ensemble is highly precise with backbone and heavy-atom root-mean-square deviation values of 0.05 ± 0.01 and 0.41 ± 0.04 Å, respectively, and it ranks as 'high resolution' based upon measures of precision and stereochemical quality (Kwan *et al.*, 2011).

Figure 6 shows an overlay of the ensemble of 20 Hd1a structures. As expected, Hd1a contains an ICK motif in which the Cys17–Cys32 disulfide bond pierces a 12-residue ring formed by the other two disulfides (Cys3–Cys18, Cys10–Cys25) and the intervening sections of peptide backbone. Thus, Hd1a contains four inter-cystine loops (numbered 1–4 in Figure 6). The dominant secondary structure is a β hairpin comprising strands β1 (residues 23–26) and β2 (residues 31–34) connected by a short hairpin loop (residues 27–30; loop 4).

Table 2

Structural statistics for the ensemble of Hd1a structures

Experimental restraints	
Interproton distance restraints	
Intra-residue	178
Sequential	168
Medium range ($i–j < 5$)	142
Long range ($i–j \geq 5$)	214
Disulfide bond restraints	9
Dihedral angle restraints (ϕ, ψ)	57
Total number of restraints per residue	21.3
RMSD to mean coordinate structure (Å)	
Backbone atoms	0.05 ± 0.01
All heavy atoms	0.41 ± 0.04
Stereochemical quality	
Residues in most favoured Ramachandran region (%)	87.9 ± 0.9
Ramachandran outliers (%)	0.0 ± 0.0
Unfavourable side chain rotamers (%)	11.1 ± 2.2
Residues with bad angles	0.0 ± 0.0
Clashscore, all atoms	0.0 ± 0.0
Overall MolProbity score (percentile)	1.89 ± 0.07(81 ± 3)

Root-mean-square deviation (RMSD) values were calculated over the well-defined regions of the structures (residues 2–35). Measures of stereochemical quality are from MolProbity (http://helix.research.duhs.duke.edu). Clashscore is the number of steric overlaps >0.4 Å per 103 atoms. All statistics are given as mean ± SD.

Discussion

High-throughput venom screens

In contrast to the diversity of Na_V channels in mammals, insects contain a single isoform. Interference with this channel has lethal consequences, making it an ideal target for insect predators such as spiders, scorpions and centipedes (King *et al.*, 2008a). As a consequence, the venoms of these arthropods are rich in Na_V channel modulators (Rodriguez De La Vega and Possani, 2005; Gurevitz *et al.*, 2007; King *et al.*, 2008a; Yang *et al.*, 2012; Gilchrist *et al.*, 2014). Since there is no evolutionary selection pressure to prevent these toxins acting on vertebrates, many spider-venom peptides also modulate the activity of mammalian Na_V channels (Nicholson and Little, 2005; Escoubas and Bosmans, 2007). However, since the level of sequence identity between insect and human Na_V channels is only 55–60% (King *et al.*, 2008a), it is difficult to predict the effect of these peptides on specific hNa_V subtypes. We therefore developed a high-throughput approach for screening spider-venom peptides directly against $hNa_V1.7$.

We took advantage of the observation that the neuroblastoma cell line SH-SY5Y expresses high levels of $Na_V1.7$ to the exclusion of most other subtypes (Vetter *et al.*, 2012). This formed the basis of a high-throughput FLIPR assay in which venoms were monitored for their ability to prevent a calcium-dependent fluorescent response induced by activation of the endogenous $hNa_V1.7$ population with veratridine, a non-specific Na_V channel agonist. This assay enabled ~90 venoms to be screened in 96-well plate format; if we conservatively estimate that each venom contains 200 peptides, then this corresponds to a rapid screen of 18 000 peptides. Scaling to 384-well plates would enable rapid screening of >350 venoms (>70 000 peptides) and minimize the amount of venom required.

Using this high-throughput FLIPR assay, we demonstrated that spider venoms are an incredibly rich source of $hNa_V1.7$ modulators with the potential to serve as leads for analgesic development. A remarkable 40% of all venoms screened putatively contain at least one inhibitor of $hNa_V1.7$. Moreover, deconvolution of 'hits' revealed that some spider venoms contain more than one $hNa_V1.7$ inhibitor (e.g. see Figure 2F).

High-throughput structure–function studies

Using our $hNa_V1.7$ screen, we discovered seven novel members of NaSpTx-F1 and focused on one of these (Hd1a) in order to develop robust methods for structure–function characterization. rHd1a potently inhibited $hNa_V1.7$ with an IC_{50} of ~110 nM, with modest or zero effect on all other subtypes except $Na_V1.1$. Since most spider-venom-derived $Na_V1.7$ modulators are gating modifiers that bind to one or more of the voltage sensors, we developed an approach that allows rapid determination of which voltage-sensor is involved in toxin binding. Competition binding experiments can be difficult to interpret because some spider-venom peptides interact with more than one voltage sensor (Bosmans *et al.*, 2008); therefore, we developed an alternative approach in which a panel of channel chimeras was created by transplanting the voltage-sensor paddles from each of the four domains of

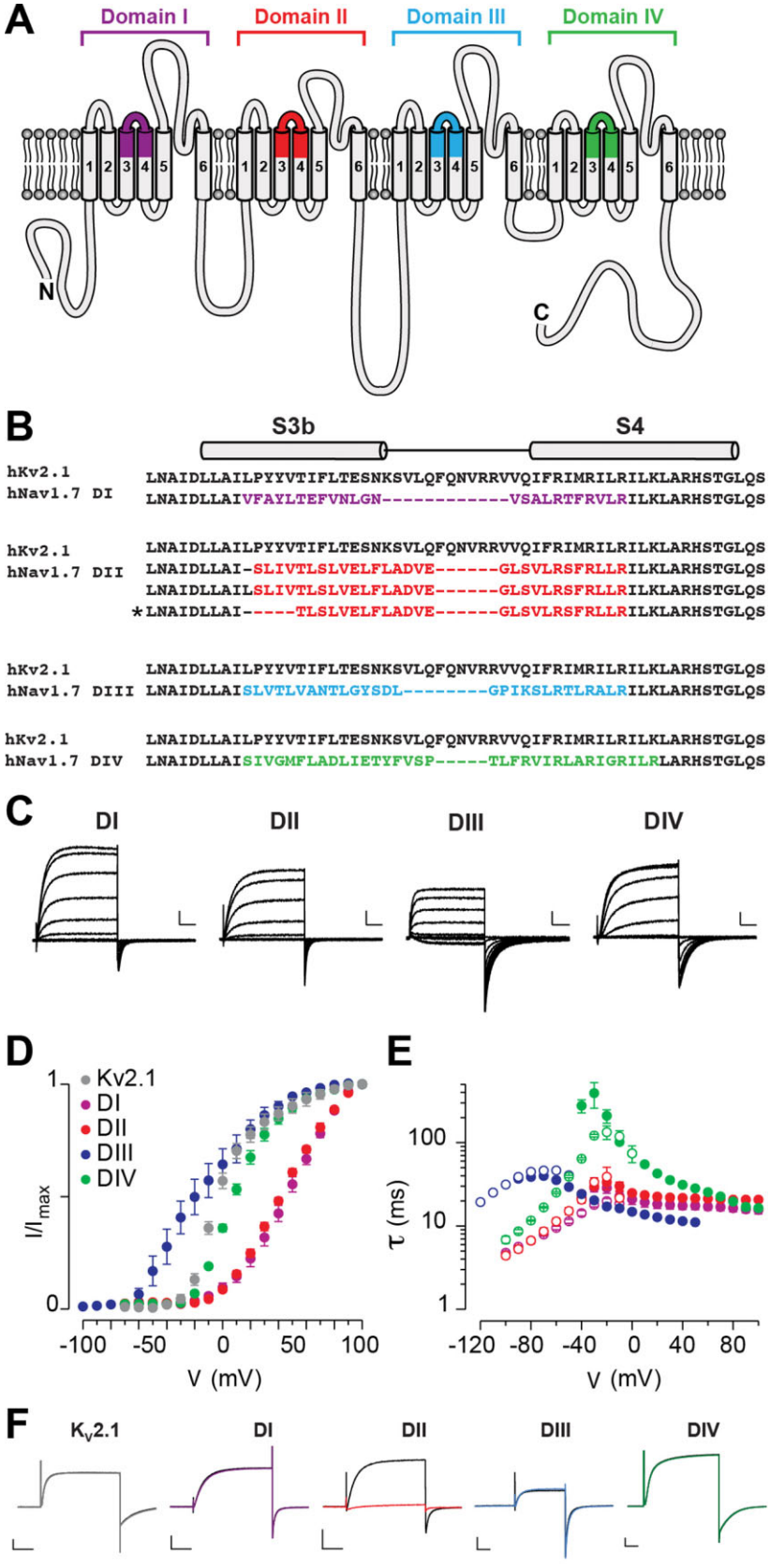
A
Domain I
Domain II
Domain III
Domain IV
N
C
B
S3b
S4
hKv2.1 LNAIDLLAILPYYVTIFLTESNKSVLQFQNVRRVVQIFRIMRILRILKLARHSTGLQS
hNav1.7 DI LNAIDLLAIVFAYLTEFVNLGN----------VSALRTFRVLRILKLARHSTGLQS
hKv2.1 LNAIDLLAILPYYVTIFLTESNKSVLQFQNVRRVVQIFRIMRILRILKLARHSTGLQS
hNav1.7 DII LNAIDLLAI-SLIVTLSLVELFLADVE------GLSVLRSFRLLRILKLARHSTGLQS
LNAIDLLAIL SLIVTLSLVELFLADVE------GLSVLRSFRLLRILKLARHSTGLQS
*LNAIDLLAI-----TLSLVELFLADVE------GLSVLRSFRLLRILKLARHSTGLQS
hKv2.1 LNAIDLLAILPYYVTIFLTESNKSVLQFQNVRRVVQIFRIMRILRILKLARHSTGLQS
hNav1.7 DIII LNAIDLLAISLVTLVANTLGYSDL--------GPIKSLRTLRALRILKLARHSTGLQS
hKv2.1 LNAIDLLAILPYYVTIFLTESNKSVLQFQNVRRVVQIFRIMRILRILKLARHSTGLQS
hNav1.7 DIV LNAIDLLAISIVGMFLADLIETYFVSP-----TLFRVIRLARIGRILRLARHSTGLQS
C
DI
DII
DIII
DIV
D
Kv2.1
DI
DII
DIII
DIV
I/Imax
V (mV)
E
τ (ms)
V (mV)
F
Kv2.1
DI
DII
DIII
DIV

Figure 5

Sensitivity of $hNa_V1.7/rK_V2.1$ paddle chimeras to rHd1a. (A) Schematic of the $hNa_V1.7$ channel showing the voltage-sensor paddle motifs (coloured segments) that were transferred from $hNa_V1.7$ to rat $K_V2.1$ ($rK_V2.1$). The paddles from domains I, II, III and IV are coloured purple, red, cyan and green respectively. (B) Sequence alignment of the paddle region of $rK_V2.1$ with the paddle motifs (S3b-S4 region) from each domain of $hNa_V1.7$. For the domain II transplant, only the chimera highlighted with an asterisk was functional. (C) Families of potassium currents for each of the $hNa_V1.7/rKv2.1$ chimeras. Scale bars: 1 μA (ordinate axis) and 50 ms (abscissa). (D) Tail current voltage-activation relationships for each of the $hNa_V1.7/rK_V2.1$ chimeras ($n = 5$; error bars denote SEM). The holding voltage was –90 mV (–120 mV for DIII) and the tail voltage was –60 mV (or –90 mV for DIII). (E) Mean time constants (τ) from single exponential fits to channel activation (filled circles) and deactivation (open circles) plotted as a function of the voltage at which the current was recorded (n = 3–5; error bars denote SEM). (F) Potassium currents elicited by depolarizations to 70 mV. Currents are shown before (black) and in the presence (coloured traces) of 1 μM rHd1a. Colours denote the domain from which the $hNa_V1.7$ paddle motif was transferred: DI paddle (purple); DII paddle (red); DIII paddle (blue); DIV paddle (green). Scale bars: 50 ms (abscissa), 1 μA (DII, DIII) and 2 μA (DI, DIV, $K_V2.1$) (ordinate axis).

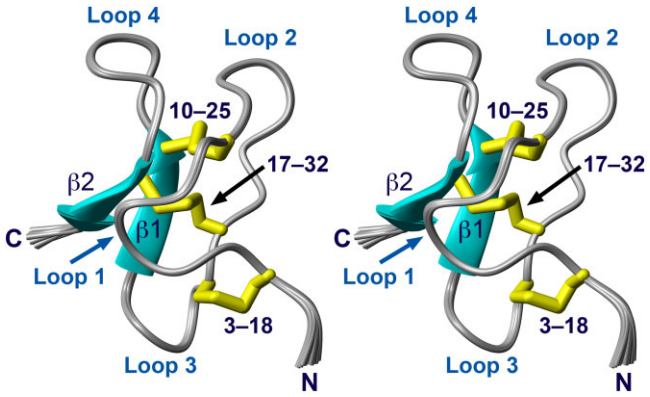

Figure 6

Ensemble of rHd1a structures. Stereoview of the ensemble of 20 rHd1a structures (PDB 2MPQ) overlaid over the backbone atoms of residues 2–35. β strands are shown in blue and the three disulfide bonds are highlighted in yellow. The four inter-cystine loops and the N- and C-termini are labelled.

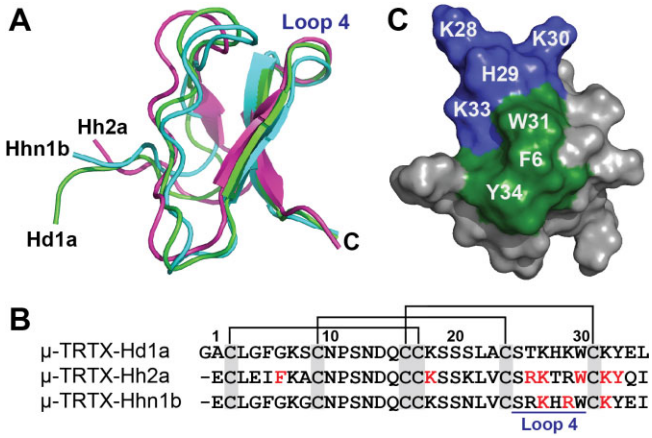

Figure 7

Structural comparison of rHd1a with characterized NaSpTx-F1 members. (A) Ribbon representation of the 3D structures of Hd1a (green, PDB 2MPQ), μ-TRTX-Hhn1b (cyan, PDB 1NIY) and μ-TRTX-Hh2a (pink, PDB 1MB6). The C-termini are labelled. (B) Alignment of the amino sequences of the three peptides. Red denotes residues that cause a reduction in inhibition of $Na_V1.7$ when mutated to alanine. Sequence numbering is with respect to μ-TRTX-Hh2a and μ-TRTX-Hhn1b. (C) Solvent accessible surface of Hd1a. Hydrophobic and basic residues are coloured green and blue, respectively, and are labelled. This view is related to that in panel (A) by a 180° rotation around the long axis of the molecule.

$hNa_V1.7$ into $rK_V2.1$ (Figure 5). This enabled us to ask whether transplantation of the $hNa_V1.7$ paddles into $rK_V2.1$ sensitizes this K_V channel to the effects of a Na_V channel toxin. Using this approach, we demonstrated that rHd1a binds exclusively to the voltage-sensor paddle from $hNa_V1.7$ domain II (Figure 5F). Hd1a joins an extensive list of animal toxins that target this paddle motif to prevent Na_v channel opening (Cestele *et al.*, 1998; Catterall *et al.*, 2007; Bosmans *et al.*, 2008; Bosmans and Swartz, 2010; Xiao *et al.*, 2011).

High-throughput screens such as the one described here are increasingly being used in venom-based drug discovery pipelines (Vetter *et al.*, 2011). This results in more lead molecules becoming available very early in the discovery pipeline than in traditional discovery programmes focussed on one or several venoms (Bosmans *et al.*, 2006). Hence, there is a need to rapidly determine the structure of several venom peptides to allow timely development of structure–activity relationships (SAR). Although NMR is the dominant approach for determining the structure of polypeptides <10 kDa (Kwan *et al.*, 2011), it suffers from low-throughput. Thus, we integrated several approaches to speed up venom-peptide structure determination. Firstly, we acquired all scalar-coupling experiments using NUS in order to expedite data acquisition and increase resolution in the indirect frequency dimensions. This enables a complete 3D/4D data set to be acquired in <5 days, and the increased digital resolution makes the spectra highly amenable to automated assignment. Secondly, we used automated NOESY assignment and structure calculation (Güntert, 2004). Together, these approaches enable high-resolution structures of excellent stereochemical quality to be determined in a highly automated fashion in 1 week, as exemplified by the structure of rHd1a reported here (Figure 6).

The structure of rHd1a is similar to that of Hhn1b and Hh2a (Figure 7A). A positively charged patch on the surface of Hhn1b is important for its inhibition of TTX-sensitive Na_V currents in DRG neurons, with mutation to alanine of residues K27, R29 and K32 resulting in >100-fold decrease in potency (Liu *et al.*, 2012). These three cationic residues are conserved in Hd1a (corresponding residues are K28, K30 and K33; Figure 7B). Extensive mutagenesis of Hh2a, which is

68% identical to Hd1a, also revealed that these charged residues are important for hNa$_V$1.7 inhibition, with a K32A mutation causing almost complete loss of activity (Minassian *et al.*, 2013; Revell *et al.*, 2013). Hydrophobic interactions with the channel are also important, as a W30A mutation caused complete loss of hNa$_V$1.7 inhibition, whereas F6A and Y33A mutations triggered major reductions in potency (Minassian *et al.*, 2013; Revell *et al.*, 2013). Interestingly, W30 and K32 are two of the few residues that are completely conserved in NaSpTx-F1 (Klint *et al.*, 2012). The mutational data are mapped onto the structure of rHd1a in Figure 7C. The functionally important hydrophobic and cationic residues form adjacent clusters that together create a contiguous surface epitope that likely represents the peptide's pharmacophore for hNa$_V$1.7.

Most of the residues important for interaction of NaSpTx-F1 peptides with hNa$_V$1.7 are located in the structurally well-conserved C-terminal region and loop 4 (Figure 7A). There are subtle sequence variations in these regions (see Table 1), and detailed SAR studies will be required to unravel the molecular determinants that underlie differences in subtype selectivity within NaSpTx-F1. The recently described tethered-toxin screening approach, which allows alanine scans to be performed without the need to produce and purify individual mutants (Gui *et al.*, 2014), should expedite such studies.

In summary, we developed a high-throughput screen for discovery of hNa$_V$1.7 modulators and used this screen to demonstrate that spider venoms are perhaps the best natural source of inhibitors of this target analgesic. We discovered seven novel members of NaSpTx-F1 using this screen. One of these toxins, rHd1a, potently inhibited hNa$_V$1.7 with a high level of selectivity over other hNa$_V$ subtypes In addition, we engineered a panel of hNa$_V$1.7/rKv2.1 channel chimeras that can be used to rapidly assess whether hNa$_V$1.7 toxins target any of the channel's voltage-sensor paddles. The venom-based drug discovery pipeline described here provides a paradigm for high-throughput screening of animal venoms against other therapeutic ion channel targets.

Acknowledgements

We thank Kenton Swartz for the K$_V$2.1 clone and agitoxin-2. Thanks to Jamie Vandenberg for the hERG clone and Ben Cristofori-Armstrong for helping with hERG experiments. Thanks to the members of the Deutsche Arachnologische Gesellschaft (DeArGe), particularly Arnd Schlosser, Gianni Sposato, Henrik Krehenwinkel, Reti Erler and Volker von Wirth, for providing spiders for milking. We acknowledge financial support from the Australian Research Council (Discovery Grant DP110103129 to G. F. K. and R. J. L.), the National Health & Medical Research Council (Principal Research Fellowships to G. F. K. and R. J. L.; Program Grant to R. J. L.), and the National Institute of Neurological Disorders and Stroke of the National Institutes of Health (Award R00NS073797 to F. B.). Access to the Australian Proteome Analysis Facility is facilitated by support from the Australian Government's National Collaborative Research Infrastructure Strategy.

Author contributions

G. F. K., R. J. L. and F. B. directed this program of research. G. F. K., R. L., I. V., V. H., J. K. K. and F. B. conceived and designed the experiments. J. K. K., J. J. S., D. R., S. Y. R., S. S., I. V., M. M., V. H. and F. B. performed the experiments: J. K. K., J. J. S., D. R., S. Y. R., S. S., M. M., F. B. and G. F. K. analysed the data. J. K. K., F. B. and G. F. K. wrote the paper.

Conflict of interest

The authors have no conflicts of interest.

References

Aggarwal SK, MacKinnon R (1996). Contribution of the S4 segment to gating charge in the *Shaker* K$^+$ channel. Neuron 16: 1169–1177.

Alabi AA, Bahamonde MI, Jung HJ, Kim JI, Swartz KJ (2007). Portability of paddle motif function and pharmacology in voltage sensors. Nature 450: 370–375.

Alexander SPH, Benson HE, Faccenda E, Pawson AJ, Sharman JL, Spedding M *et al.* (2013). The Concise Guide to PHARMACOLOGY 2013/14: Ion channels. Br J Pharmacol 170: 1607–1651.

Bosmans F, Swartz KJ (2010). Targeting voltage sensors in sodium channels with spider toxins. Trends Pharmacol Sci 31: 175–182.

Bosmans F, Rash L, Zhu S, Diochot S, Lazdunski M, Escoubas P *et al.* (2006). Four novel tarantula toxins as selective modulators of voltage-gated sodium channel subtypes. Mol Pharmacol 69: 419–429.

Bosmans F, Martin-Eauclaire MF, Swartz KJ (2008). Deconstructing voltage sensor function and pharmacology in sodium channels. Nature 456: 202–208.

Bosmans F, Puopolo M, Martin-Eauclaire MF, Bean BP, Swartz KJ (2011). Functional properties and toxin pharmacology of a dorsal root ganglion sodium channel viewed through its voltage sensors. J Gen Physiol 138: 59–72.

Cabrita LD, Dai W, Bottomley SP (2006). A family of *E. coli* expression vectors for laboratory scale and high throughput soluble protein production. BMC Biotech 6: 12.

Catterall WA, Goldin AL, Waxman SG (2005). International Union of Pharmacology. XLVII. Nomenclature and structure-function relationships of voltage-gated sodium channels. Pharmacol Rev 57: 397–409.

Catterall WA, Cestele S, Yarov-Yarovoy V, Yu FH, Konoki K, Scheuer T (2007). Voltage-gated ion channels and gating modifier toxins. Toxicon 49: 124–141.

Cestele S, Qu Y, Rogers JC, Rochat H, Scheuer T, Catterall WA (1998). Voltage sensor-trapping: enhanced activation of sodium channels by β-scorpion toxin bound to the S3-S4 loop in domain II. Neuron 21: 919–931.

Chanda B, Bezanilla F (2002). Tracking voltage-dependent conformational changes in skeletal muscle sodium channel during activation. J Gen Physiol 120: 629–645.

Chen VB, Arendall WB 3rd, Headd JJ, Keedy DA, Immormino RM, Kapral GJ *et al.* (2010). MolProbity: all-atom structure validation for macromolecular crystallography. Acta Crystallogr D Biol Crystallogr 66: 12–21.

Cheng X, Dib-Hajj SD, Tyrrell L, Te Morsche RH, Drenth JP, Waxman SG (2011). Deletion mutation of sodium channel $Na_V1.7$ in inherited erythromelalgia: enhanced slow inactivation modulates dorsal root ganglion neuron hyperexcitability. Brain 134: 1972–1986.

Cox JJ, Reimann F, Nicholas AK, Thornton G, Roberts E, Springell K *et al*. (2006). An *SCN9A* channelopathy causes congenital inability to experience pain. Nature 444: 894–898.

Duan G, Xiang G, Zhang X, Yuan R, Zhan H, Qi D (2013). A single-nucleotide polymorphism in *SCN9A* may decrease postoperative pain sensitivity in the general population. Anesthesiology 118: 436–442.

Escoubas P, Bosmans F (2007). Spider peptide toxins as leads for drug development. Expert Opin Drug Discov 2: 823–835.

Escoubas P, Sollod B, King GF (2006). Venom landscapes: mining the complexity of spider venoms via a combined cDNA and mass spectrometric approach. Toxicon 47: 650–663.

Estacion M, Dib-Hajj SD, Benke PJ, Te Morsche RH, Eastman EM, Macala LJ *et al*. (2008). $Na_V1.7$ gain-of-function mutations as a continuum: A1632E displays physiological changes associated with erythromelalgia and paroxysmal extreme pain disorder mutations and produces symptoms of both disorders. J Neurosci 28: 11079–11088.

Fertleman CR, Baker MD, Parker KA, Moffatt S, Elmslie FV, Abrahamsen B *et al*. (2006). *SCN9A* mutations in paroxysmal extreme pain disorder: allelic variants underlie distinct channel defects and phenotypes. Neuron 52: 767–774.

Frech GC, Vandongen AM, Schuster G, Brown AM, Joho RH (1989). A novel potassium channel with delayed rectifier properties isolated from rat brain by expression cloning. Nature 340: 642–645.

Garcia ML, Garcia-Calvo M, Hidalgo P, Lee A, Mackinnon R (1994). Purification and characterization of three inhibitors of voltage-dependent K^+ channels from *Leiurus quinquestriatus* var. *hebraeus* venom. Biochemistry 33: 6834–6839.

Gaskin DJ, Richard P (2012). The economic costs of pain in the United States. J Pain 13: 715–724.

Gilchrist J, Olivera BM, Bosmans F (2014). Animal toxins influence voltage-gated sodium channel function. Handb Exp Pharmacol 221: 203–229.

Gui J, Liu B, Cao G, Lipchik AM, Perez M, Dekan Z *et al*. (2014). A tarantula-venom peptide antagonizes the TRPA1 nociceptor ion channel by binding to the S1-S4 gating domain. Curr Biol 24: 473–483.

Gurevitz M, Karbat I, Cohen L, Ilan N, Kahn R, Turkov M *et al*. (2007). The insecticidal potential of scorpion β-toxins. Toxicon 49: 473–489.

Güntert P (2004). Automated NMR structure calculation with CYANA. Methods Mol Biol 278: 353–378.

Herzig V, Wood DL, Newell F, Chaumeil PA, Kaas Q, Binford GJ *et al*. (2011). ArachnoServer 2.0, an updated online resource for spider toxin sequences and structures. Nucl Acids Res 39: D653–D657.

Horn R, Ding S, Gruber HJ (2000). Immobilizing the moving parts of voltage-gated ion channels. J Gen Physiol 116: 461–476.

Kapust RB, Tozser J, Copeland TD, Waugh DS (2002). The P1′ specificity of tobacco etch virus protease. Biochem Biophys Res Commun 294: 949–955.

King GF (2007). Modulation of insect Ca_V channels by peptidic spider toxins. Toxicon 49: 513–530.

King GF, Vetter I (2014). No gain, no pain: $Na_V1.7$ as an analgesic target. ACS Chem Neurosci 5: 749–751.

King GF, Escoubas P, Nicholson GM (2008a). Peptide toxins that selectively target insect Na_V and Ca_V channels. Channels 2: 100–116.

King GF, Gentz MC, Escoubas P, Nicholson GM (2008b). A rational nomenclature for naming peptide toxins from spiders and other venomous animals. Toxicon 52: 264–276.

Klint JK, Senff S, Rupasinghe DB, Er SY, Herzig V, Nicholson GM *et al*. (2012). Spider-venom peptides that target voltage-gated sodium channels: pharmacological tools and potential therapeutic leads. Toxicon 60: 478–491.

Klint JK, Senff S, Saez NJ, Seshadri R, Lau HY, Bende NS *et al*. (2013). Production of recombinant disulfide-rich venom peptides for structural and functional analysis via expression in the periplasm of *E. coli*. PLoS ONE 8: e63865.

Kwan AH, Mobli M, Gooley PR, King GF, Mackay JP (2011). Macromolecular NMR spectroscopy for the non-spectroscopist. FEBS J 278: 687–703.

Liu Y, Li D, Wu Z, Li J, Nie D, Xiang Y *et al*. (2012). A positively charged surface patch is important for hainantoxin-IV binding to voltage-gated sodium channels. J Pept Sci 18: 643–649.

Minassian NA, Gibbs A, Shih AY, Liu Y, Neff RA, Sutton SW *et al*. (2013). Analysis of the structural and molecular basis of voltage-sensitive sodium channel inhibition by the spider toxin huwentoxin-IV (μ-TRTX-Hh2a). J Biol Chem 288: 22707–22720.

Mobli M, Maciejewski MW, Gryk MR, Hoch JC (2007). An automated tool for maximum entropy reconstruction of biomolecular NMR spectra. Nat Meth 4: 467–468.

Mobli M, Stern AS, Bermel W, King GF, Hoch JC (2010). A non-uniformly sampled 4D HCC(CO)NH-TOCSY experiment processed using maximum entropy for rapid protein sidechain assignment. J Magn Reson 204: 160–164.

Nicholson GM, Little MJ (2005). Spider neurotoxins targeting voltage-gated sodium channels. Toxin Rev 24: 315–345.

Pallaghy PK, Nielsen KJ, Craik DJ, Norton RS (1994). A common structural motif incorporating a cystine knot and a triple-stranded β-sheet in toxic and inhibitory polypeptides. Protein Sci 3: 1833–1839.

Pawson AJ, Sharman JL, Benson HE, Faccenda E, Alexander SP, Buneman OP *et al*.; NC-IUPHAR (2014). The IUPHAR/BPS Guide to PHARMACOLOGY: an expert-driven knowledgebase of drug targets and their ligands. Nucl. Acids Res. 42 (Database Issue): D1098–106.

Reeder JE, Byler TK, Foster DC, Landas SK, Okafor H, Stearns G *et al*. (2013). Polymorphism in the *SCN9A* voltage-gated sodium channel gene associated with interstitial cystitis/bladder pain syndrome. Urology 81: 210, e1–210.e4.

Reimann F, Cox JJ, Belfer I, Diatchenko L, Zaykin DV, Mchale DP *et al*. (2010). Pain perception is altered by a nucleotide polymorphism in *SCN9A*. Proc Natl Acad Sci U S A 107: 5148–5453.

Renicke C, Spadaccini R, Taxis C (2013). A tobacco etch virus protease with increased substrate tolerance at the P1′ position. PLoS ONE 8: e67915.

Revell JD, Lund PE, Linley JE, Metcalfe J, Burmeister N, Sridharan S *et al*. (2013). Potency optimization of huwentoxin-IV on $hNa_V1.7$: a neurotoxin TTX-S sodium-channel antagonist from the venom of the Chinese bird-eating spider *Selenocosmia huwena*. Peptides 44: 40–46.

Rodriguez De La Vega RC, Possani LD (2005). Overview of scorpion toxins specific for Na^+ channels and related peptides: biodiversity, structure-function relationships and evolution. Toxicon 46: 831–844.

Ruta V, MacKinnon R (2004). Localization of the voltage-sensor toxin receptor on KvAP. Biochemistry 43: 10071–10079.

Seoh SA, Sigg D, Papazian DM, Bezanilla F (1996). Voltage-sensing residues in the S2 and S4 segments of the *Shaker* K^+ channel. Neuron 16: 1159–1167.

Sheets MF, Kyle JW, Kallen RG, Hanck DA (1999). The Na channel voltage sensor associated with inactivation is localized to the external charged residues of domain IV, S4. Biophys J 77: 747–757.

Shen Y, Delaglio F, Cornilescu G, Bax A (2009). TALOS+: a hybrid method for predicting protein backbone torsion angles from NMR chemical shifts. J Biomol NMR 44: 213–223.

Sousa SR, Vetter I, Ragnarsson L, Lewis RJ (2013). Expression and pharmacology of endogenous Ca_V channels in SH-SY5Y human neuroblastoma cells. PLoS ONE 8: e59293.

Swartz KJ, MacKinnon R (1997). Hanatoxin modifies the gating of a voltage-dependent K^+ channel through multiple binding sites. Neuron 18: 665–673.

Theile JW, Jarecki BW, Piekarz AD, Cummins TR (2011). Nav1.7 mutations associated with paroxysmal extreme pain disorder, but not erythromelalgia, enhance Navβ4 peptide-mediated resurgent sodium currents. J Physiol 589: 597–608.

Vetter I, Davis JL, Rash LD, Anangi R, Mobli M, Alewood PF *et al*. (2011). Venomics: a new paradigm for natural products-based drug discovery. Amino Acids 40: 15–28.

Vetter I, Mozar CA, Durek T, Wingerd JS, Alewood PF, Christie MJ *et al*. (2012). Characterisation of Na_V types endogenously expressed in human SH-SY5Y neuroblastoma cells. Biochem Pharmacol 83: 1562–1571.

Xiao Y, Bingham JP, Zhu W, Moczydlowski E, Liang S, Cummins TR (2008). Tarantula huwentoxin-IV inhibits neuronal sodium channels by binding to receptor site 4 and trapping the domain II voltage sensor in the closed configuration. J Biol Chem 283: 27300–27313.

Xiao Y, Jackson JO 2nd, Liang S, Cummins TR (2011). Common molecular determinants of tarantula huwentoxin-IV inhibition of Na^+ channel voltage-sensors in domains II and IV. J Biol Chem 286: 27301–27310.

Yang S, Liu Z, Xiao Y, Li Y, Rong M, Liang S *et al*. (2012). Chemical punch packed in venoms makes centipedes excellent predators. Mol Cell Proteomics 11: 640–650.

Yang Y, Wang Y, Li S, Xu Z, Li H, Ma L *et al*. (2004). Mutations in *SCN9A*, encoding a sodium channel alpha subunit, in patients with primary erythermalgia. J Med Genet 41: 171–174.

Supporting information

Additional Supporting Information may be found in the online version of this article at the publisher's web-site:

http://dx.doi.org/10.1111/bph.13081

Figure S1 Voltage-dependence of Na_V channel inhibition by rHd1a. (A) Inhibition of $Na_V1.7$-mediated currents by rHd1a is not voltage-dependent from –25 to 0 mV (n = 3–4; error bars denote SEM). Currents were evoked from a holding potential of –90 mV, stepping from –70 to 0 mV in 5 mV increments. (B) Selectivity of rHd1a is not voltage-dependent from –25 to 0 mV. I/I_0 in the presence of 1 μM rHd1a for $hNa_V1.2$, $hNa_V1.3$, $hNa_V1.5$ and $hNa_V1.7$ (n = 3–4; error bars denote SEM). Currents were evoked from a holding potential of –90 mV, stepping from –70 to 0 mV in 5 mV increments.
Figure S2 Effect of rHd1a on $hNa_V1.7$ inactivation time constants. Time constant (|) for inactivation of $hNa_V1.7$ in the absence (black) or presence (red) of 1 μM rHd1a (n = 5–7; error bars denote SEM). The rate of inactivation is slowed in the presence of rHd1a. Currents were evoked from a holding potential of –90 mV, stepping from –70 to +20 mV in 5 mV increments.
Figure S3 Effect of rHd1a on human ERG channels (hERG, $K_v11.1$). The current–voltage (I–V) relationship for hERG was measured by applying 2 s pulses to test potentials ranging from –70 to +40 mV in 10 mV increments and then by a repolarizing step to –70 mV for 1 s. Tail currents are plotted as a function of voltage and fitted to a Boltzmann equation (n = 6; error bars denote SEM). There was no significant difference between control currents (black) and those following addition of 1 μM rHd1a (red).
Figure S4 Effect of rHd1a on $hNa_V1.9/rK_v2.1$ chimeras. Tail current–voltage relationships for a panel of $hNa_V1.9/rK_v2.1$ chimeras obtained before (black) or after (red) addition of 1 μM rHd1a (n = 5–8; error bars denote SEM). These chimeras were constructed by transplanting the S3b-S4 paddle from each domain of $hNa_V1.9$ (DI, DII, DIII and DIV, as indicated) into $rK_v2.1$; construction and characterization of these chimeras was reported previously.[1] The holding voltage was –90 mV (or –120 mV for DII) and the tail voltage was –70 mV for the DI (panel A), –90 mV for DII (panel B), –60 mV for DIII (panel C) and –80 mV for DIV (panel D) chimeras. rHd1a had no effect on any of the chimeric channels.
Figure S5 Fully assigned 2D ^1H-^{15}N-HSQC spectrum of Hd1a. Horizontal lines connect peaks corresponding to the two side chain NH groups of N11, N14, and Q16. The peak from the indole side chain of W31 is also labelled. All other peaks are from backbone amide groups. The ^1H-^{15}N-HSQC spectrum is missing resonances from the backbone amide groups of K30 and W31, but they were present in 3D ^{15}N- and ^{13}C-edited HSQC-NOESY spectra.
Table S1 List of species from which venom was obtained for this study.